International Journal of Heat and Mass Transfer 68 (2014) 456–465

Contents lists available at ScienceDirect

International Journal of Heat and Mass Transfer

journal homepage: www.elsevier.com/locate/ijhmt

On using film boiling to thermally decompose liquid organic chemicals: Application to ethyl acetate as a model compound

Wei-Chih Kuo [a,*], C. Thomas Avedisian [a], Kyung Hwa Choi [a], Wing Tsang [b]

[a] Sibley School of Mechanical and Aerospace Engineering, Cornell University, Ithaca, NY 14853, USA
[b] Physical and Chemical Properties Division, National Institute of Standards and Technology, Gaithersburg, MD 20899, USA

ARTICLE INFO

Article history:
Received 9 December 2012
Received in revised form 19 August 2013
Accepted 21 August 2013

Keywords:
Film boiling
Thermal decomposition
Pyrolysis
Ethyl acetate
Critical heat flux (CHF)
Leidenfrost point

ABSTRACT

Film boiling on a horizontal tube is used to study the thermal decomposition of ethyl acetate. The decomposition process is driven by the high surface temperatures that are typical of the film boiling regime that can promote chemical change of superheated vapors in a low temperature liquid. The decomposition products are carried away from the tube by vapor bubbles formed at the top of the tube that then percolate through the system. For the experiments reported here, the bulk liquid is stagnant, the liquid is slightly subcooled, and bubble transport is entirely by buoyancy.

The results show that the primary decomposition products are acetic acid and ethylene in proportions consistent with the accepted unimolecular decomposition pathway for ethyl acetate. While ethylene is a non-condensable product gas, acetic acid is miscible in ethyl acetate and small amounts of it were detected in the bulk liquid after four hours of operation. The resulting binary (ethyl acetate/acetic acid) phase equilibrium behavior of the reactant pool contributed to trace amounts of carbon dioxide and methane being found in the product gas from acetic acid decomposition that had preferentially vaporized in the film.

The minimum film boiling temperature of ethyl acetate was measured to be approximately 711 K. Up to about 1000 K the product yields showed a comparatively small variation with average tube temperature, while above 1000 K the exhaust gas flow rate was substantial and increased in an approximately linear fashion with tube temperature. Methane and carbon dioxide were also detected in the product stream owing to acetic acid decomposition, though the amounts were comparatively small. The results show the viability for film boiling to promote decomposition in a controlled way to products consistent with those expected from the reactant molecule.

1. Introduction

Chemical conversion of condensed phase organic molecules to lighter fractions requires pre-vaporizing the reactant, which is typically accomplished in a process separate from the reactor, after which the reactant gas is transported to the high temperature reaction environment (e.g., flow [1], opposed jet [2,3], jet-stirred [4], and monolith chemical [5,6] reactor configurations, etc.). Alternative concepts have been developed that more closely couple pre-vaporization and transport. A number of the designs employ partial catalytic oxidation to provide for autothermal operation without external heat input owing to the exothermicity of the oxidative conversion process. For example, one design involves partial oxidation inside a tube of a gaseous reactant flowing within a porous platinum support positioned in the tube [7]. Air is pumped through the porous tube on one side and gaseous reactant is supplied by vaporization of the reactant liquid on the other. Other concepts that use vaporization of a liquid to transport the reactant gas include spray injection of a hydrocarbon into a cylindrical tube to coat the tube walls with the liquid, and subsequent evaporation of the liquid film by external heat addition to the tube [8–10]. The reactant gases that flow through a catalyst honeycomb are then partially oxidized.

Vaporization of droplets that impinge on a surface has also been used as a means to develop a gaseous reactant such that the droplets are levitated above the surface as in the classic Leidenfrost phenomena [12]. The vapors underneath the droplet may react homogeneously in the vapor film that separates the liquid from the solid, or the vapors may flow into a porous catalytic substrate [13,14] and heterogeneously react on the surface of the pores to form products [11]. This latter process also forms the basis of a droplet impingement reactor concept described by Varady [15].

The present paper employs a reactor that relies on evaporation of a liquid to both provide the reactant gas supply and to define the

* Corresponding author.
E-mail address: wk253@cornell.edu (W.-C. Kuo).

0017-9310/$ - see front matter © 2013 Elsevier Ltd. All rights reserved.
http://dx.doi.org/10.1016/j.ijheatmasstransfer.2013.08.054

Nomenclature

A_i	coefficient of the trend line in Fig. 10
a_i	coefficient of the calibration curve (mL min^{-1} V^{-2})
B_i	coefficient of the trend line in Fig. 10 (K)
b_i	coefficient of the calibration curve (mL min^{-1} V^{-1})
C_i	coefficient of the trend line in Fig. 10
C_{pi}	product concentration of species i (M)
C_R	reactant concentration (M)
c_i	coefficient of the calibration curve (mL min^{-1})
d_o	outer diameter of heater tube (m)
d_i	inner diameter of heater tube (m)
E_a	activation energy (cal mole^{-1})
g	gravity (m s^{-2})
h_{fg}	heat of vaporization (kJ kg^{-1})
H_c	heat of combustion (kJ kg^{-1})
I	current (A)
K	reaction rate (s^{-1})
L	tube length (m)
N	number of product gas species
$\dot{N}$	molar flow rate of a mixture gas (mole s^{-1})
$\dot{n}_i$	molar flow rate of the individual non-condensable gases (mole s^{-1})
P	Pressure (atm)
Q_{in}	power supplied to the heater tube (W)
R	radius of the heater tube (m)
R'	characteristic length for horizontal cylinders
$\bar{R}$	gas constant (cal mole^{-1} K^{-1})
t	time (s)
T	temperature (K)
T_b	normal boiling temperature (K)
T_w	tube wall temperature (K)
y_i	molar fraction of a single gas in the product gas stream
V	flow meter output (V)
$\dot{V}$	volumetric flow rate of a mixture gas (mL min^{-1})
$\dot{S}_i$	calibration relation of a single gas (mL min^{-1})
q''	heat flux (W m^{-2})
$q''_{\max}$	critical heat flux (W m^{-2})

Greek letters

δ	vapor film thickness (m)
ρ	electrical resistivity (μΩ m)
ρ_l	liquid density (kg m^{-3})
ρ_v	gas density (kg m^{-3})
σ	surface tension (N m^{-1})

actual reactor volume in a sort of self-assembled manner. The transport dynamics of such a reactor were analyzed [16,17], and subsequently shown to be capable of converting several organic species to products [18,19] including methanol and aqueous ethylene glycol mixtures to synthesis gas (a mixture of CO and H_2) as the primary product. Carbon formation was noted for the pure organic while it was reduced significantly for the aqueous mixtures. Both catalytic (surface reaction on platinum and nickel catalysts) and homogeneous gas phase processes characterized the conversion process.

The complexity of the molecules thus far examined by film boiling has made it a challenge to infer the reaction pathways from measurement of the exhaust gas composition. While ethylene glycol and methanol decompose to synthesis gas as the primary products, detection of methane and carbon dioxide in the exhaust gas, as well as carbon formation on the heater surface suggests additional conversion steps.

In the present study, the thermal decomposition of a model compound for which decomposition is expected to be particularly simple is examined: ethyl acetate (EA, $CH_3COOC_2H_5$, normal boiling point of 350 K). EA is known to decompose in a single step into two products (acetic acid and ethylene) with a known rate constant [20–24] so that measurements of product yields should ultimately be valuable for validating models of film boiling (e.g., [25–29]) to include chemical reactions [16,17]. In addition, the limited number of product gas species for ethyl acetate decomposition facilitates developing calibration correlations in the experiment for converting electronic information (e.g., voltage) from digital flow meter output to flow rates. EA also has several industrial applications, including its use as a solvent and as a hardener in paints.

Non-oxidative (pyrolytic) conversion of ethyl acetate is being examined, so that the conversion process requires a net energy input to maintain a steady decomposition process. This is accomplished in the present study by employing an electrically heated horizontal tube as the geometry used to support film boiling and the reactor volume (the vapor film). The tube is mounted in a pool of the reactant liquid which is maintained close to its saturation temperature. Film boiling is established by heating the immersed tube to promote a natural progression of heat transfer modes as the liquid transitions from single phase convection to nucleate boiling and ultimately through the critical heat flux (CHF) condition to film boiling where a stable vapor film surrounds the tube. Fig. 1 is a schematic of this configuration. In film boiling, the insulating effect of the vapor produces a large temperature drop between the high tube surface temperature and the comparatively colder liquid/vapor interface which is at the saturation temperature. The conversion process occurs within the vapor film at rates commensurate with the local temperature and the concentration of reactant gases.

Gases flowing in the film collect at the top of the tube where bubbles form, detach and percolate through the liquid pool (under

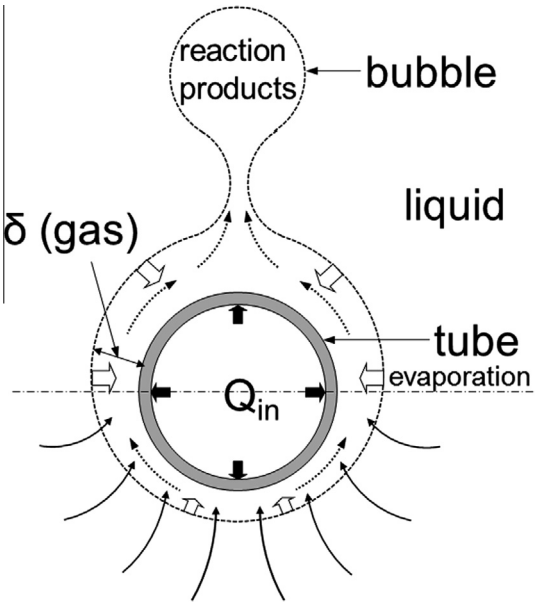

Fig. 1. Schematic cross-sectional view of film boiling on a horizontal tube.

the action of gravity in the current design). The bubbles contain the product gases and reactants not converted. The exhaust gas stream is subsequently analyzed to identify the product gases, their fractional amount and the total flow rate. Residence times for the reaction process by film boiling are on the order of milliseconds for tubes with diameters greater than several millimeters [16], which can be reduced by using smaller diameter tubes (e.g., wires).

The experimental design used to establish film boiling, measure product yields identify the species produced is presented in the next section, followed by a discussion of the EA decomposition chemistry and the results.

2. Experimental design and procedures

Fig. 2 is a schematic of the apparatus. The design includes a horizontal electrically heated tube with provision for monitoring the bulk liquid temperature, the exhaust gas flow rate, and gas and liquid compositions. The apparatus includes a chamber that contains the reactant liquid and tube on which film boiling is established, an array of condensers (that includes a dry ice/acetone mixture in series with a cold trap (a mixture of ice and water) to separate condensable and non-condensable products; the condensable species were allowed to return to the liquid reactant under gravity), and hardware for data acquisition and chemical detection. A brief discussion of the design and procedures is given below (additional details are discussed elsewhere [18,19,30]).

The chamber is comprised of a 150 mm I.D., 4.62 L capacity glass cylinder filled with 4.0 L of the test liquid (EA). Metal flanges are used to close off the ends, and they incorporate feed-through fittings for thermocouples and the power copper busses that provide electrical energy to the horizontally mounted tube on which film boiling is established. Four immersion heaters (Wattco, WC20303001) are mounted in the bottom cover flange to maintain the EA liquid close to its saturation temperature.

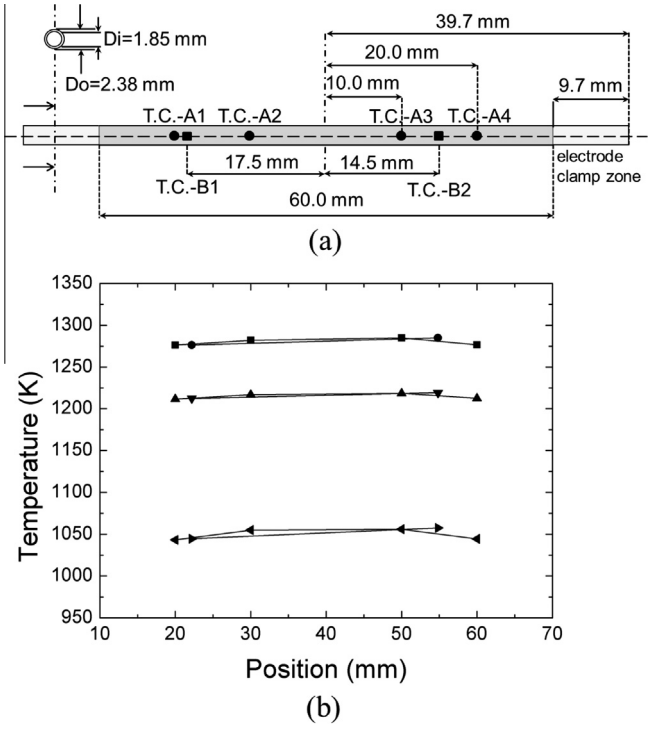

Fig. 3. (a) Heater tube dimensions with different configurations of thermocouple positions: T.C-A and T.C.-B. (b) Temperature distribution along the tube with three heat flux settings. (■: 569.3 kW/m^2, T_{avg} = 1280.0 K; ●: 572.3 kW/m^2, T_{avg} = 1280.6 K; ▲: 470.1 kW/m^2, T_{avg} = 1214.8 K; ▼: 479.4 kW/m^2, T_{avg} = 1215.7 K; ◀: 339.5 kW/m^2, T_{avg} = 1049.6 K; ▶: 336.1 kW/m^2, T_{avg} = 1051.0 K).

The heater tube assembly is shown in Fig. 3(a). It consists of a thin-walled nickel alloy tube (Inconel 600, MicroGroup, 600F10093X010SL, melting point of 1686 K) with a ceramic tube

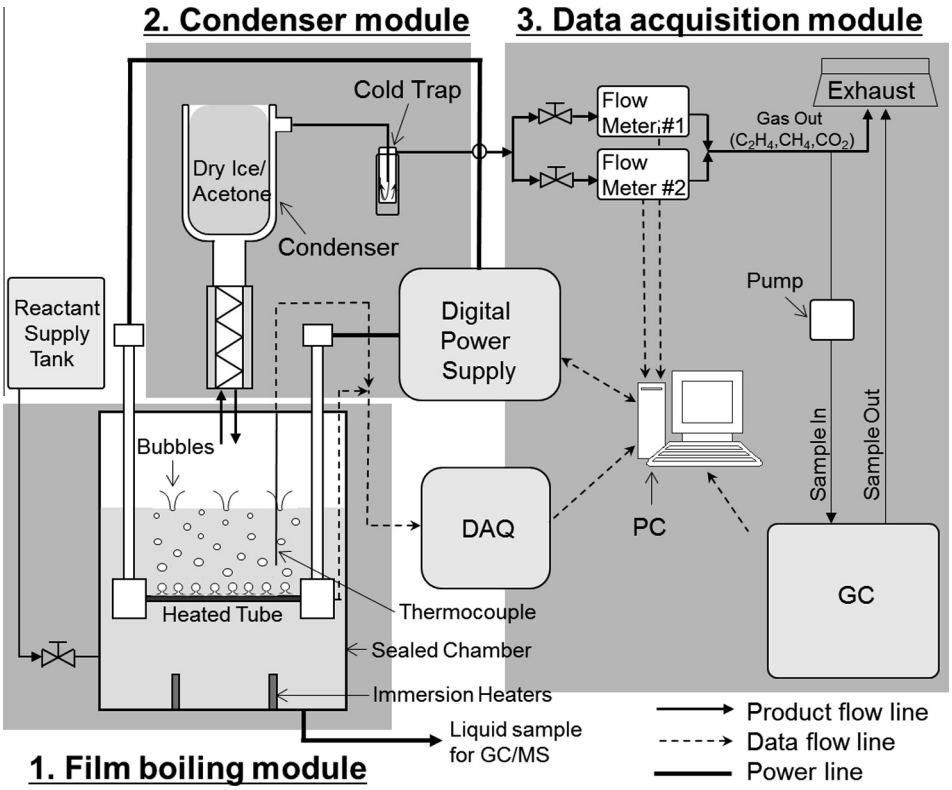

Fig. 2. Schematic of apparatus.

insert (Omega, ORX-132116) for structural support to minimize sagging of the tube as it is heated to near its melting point. The insert also provides electrical shielding of the four thermocouples (Omega, KMQXL-010G) positioned inside of it at the locations shown in Fig. 3(a) that were used to monitor the tube temperature at each power setting imposed. Four thermocouples were employed at the locations shown in Fig. 3(a), but two thermocouples were found to work just as well (at locations T.C.-B1 and T.C.-B2 in Fig. 3(a)) with nearly the same results. Fig. 3(b) shows a representative temperature distribution along the tube axis at the indicated heat fluxes when two and four thermocouples are used. Corrections for temperature drop in the radial direction from the tube center and outer surface were shown to be negligible for the conditions employed here [30].

With the design of Fig. 2, condensed liquid may reflux to the pool. To identify dissolved products that may be present in the liquid pool as a result of this effect, the liquid was sampled periodically and analyzed by a gas chromatograph/mass spectrometer (GC/MS) system (Agilent, 5973 N) with an electron impact detector (EID) that incorporates NIST spectral libraries. Results are discussed in Section 4.2.

The data acquisition section consists of two flow meters in parallel, a programmable digital power supply, a personal computer, and a gas chromatograph. The digital power supply (Aglient, 6681A) provides direct current to the heater tube at levels controlled by a LabVIEW program that also monitors thermocouple and flow meter outputs.

To develop film boiling, the tube is first immersed into the liquid pool. Power to the immersion heaters is then applied to raise the liquid temperature to near saturation conditions after which the tube is heated in steps (with voltage increments of 0.1 V; the current is automatically adjusted by the power supply commensurate with the electrical resistance of the tube). At each voltage increment, thermal conditions are allowed to stabilize for 5 minutes. The heat transfer modes transition from single phase convection, to nucleate boiling, the CHF, and ultimately to film boiling. The tube did not sustain any damage associated with the insulating effect of the EA vapors as the heat transfer mode transitioned from CHF to film boiling. The approach of establishing film boiling that begins with the tube initially in the liquid before power is applied is simpler than the one used in prior studies [18,19,30] that was developed to avoid burnout for fluids with a higher boiling point on transition from CHF to film boiling. The EA properties were more favorable for this simpler approach to developing film boiling, and in no case did burnout occur when developing film boiling of EA.

After film boiling is established, the tube surface temperature is varied to promote thermal decomposition within the vapor film. At each tube temperature, the bulk liquid temperatures, current through the tube, exhaust gas flow rates, identification of the species present and their fractional amounts in the exhaust line are measured. Concurrently, the liquid was sampled periodically for off-line GC/MS to monitor the composition.

Exhaust gas flow rates were measured using two flow meters (#1 and #2 in Fig. 2) that cover complementary ranges for enhanced precision (i.e., Omega Engineering Co., models FMA-A2309 and FMA-4310 digital flow meters). They were installed in parallel, with the flow stream directed to the meter best matched to the flow rate corresponding to the tube temperature and input power imposed. The flow meters were calibrated against a standard flow meter (Bios International Corp., Definer 220 flow meter), and conversion of the voltage to flow rate was accomplished by a calibration described in Appendix A. The exhaust gas composition and fractional amounts of species in the stream were measured by directing a small amount of the product gas (30 mL/min) into a gas chromatograph (Gow-Mac Instruments, Series 600-TCD gas chromatograph).

The heat flux dissipated by the tube of length L for each voltage input is determined from the measured current through the tube and its electrical resistivity (neglecting axial conduction effects [30]) as

$$q'' = I^2 \frac{4\rho}{\pi^2 d_o (d_o^2 - d_i^2)}, \tag{1}$$

where the electrical resistivity for Inconel 600 is [31]

$$\rho = 0.4763 + (5.27 \times 10^{-3})T - (1.95 \times 10^{-5})T^2 + (3.56 \times 10^{-8})T^3 - (3.23 \times 10^{-11})T^4 + (1.35 \times 10^{-14})T^5 - (1.89 \times 10^{-18})T^6 \tag{2}$$

This flux will be slightly lower from the flux determined by the measured voltage and current because of the small contributions from the support electrodes and lead wires.

Flow rate and tube surface temperature measurements exhibited low level fluctuations over the sample interval at each power setting. Fig. 4 shows representative flow rate fluctuations for an average tube surface temperature of 1252 K and an input power of 528 kW/m^2. In this case the reactant liquid had evolved into a

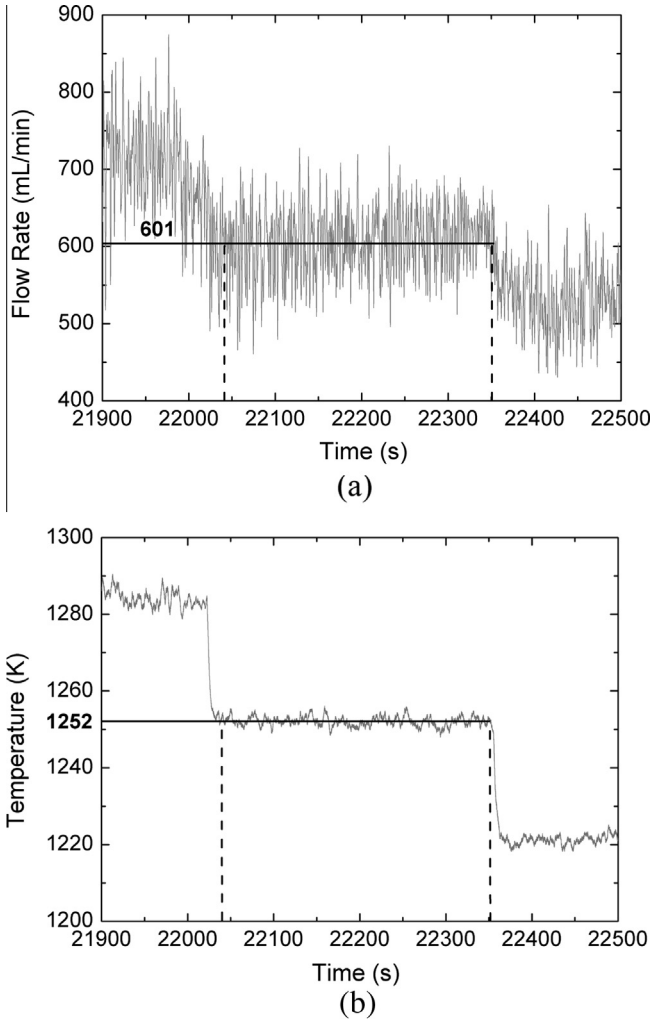

Fig. 4. Fluctuations of (a) exhaust gas flow rate and (b) tube temperature at location T.C.-B1 in Fig. 3(a) with a corresponding heat flux of 528 kW/m^2. The average value is indicated over the sampling interval.

mixture of EA and acetic acid owing to acetic acid being a major product of EA decomposition (see Section 3). Due to these fluctuations, the surface temperatures and flow rates presented in Section 4 are averaged over the sample interval (cf, the horizontal lines in Fig. 4).

The flow rate and surface temperature fluctuations are thought to arise from bubbling action in the liquid pool. This consideration was confirmed by noting that no fluctuations were observed in the single phase regime of the boiling curve. Bubbles in the condenser associated with phase change of the dry ice may also have contributed to flow rate fluctuations. However, it was determined that the contribution of bubbling action in the condenser to the fluctuating flow rate amounted to about a 3% correction in the flow rate. Because of the lack of precision of knowing the precise cause of the flow rate fluctuations, the results presented in Section 4.2 are for flow rates as measured directly.

3. Decomposition chemistry of ethyl acetate

Pyrolysis of EA is expected to be a unimolecular process with two major products forming: acetic acid (CH_3COOH) and ethylene (C_2H_4) [20],

$$CH_3COOC_2H_5 \xrightarrow{K_1} CH_3COOH + C_2H_4 \quad (3)$$

with known rate constant, K_1 [20–24]. Acetic acid is soluble in EA. The experimental design described in Section 2 has no special provision to prevent refluxing (e.g., by dripping) of condensable soluble species into the chamber. As a result, the liquid pool will be transformed over time from a single component reactant (EA) to a miscible mixture containing acetic acid and other condensable and soluble products. For example, Fig. 5 shows the evolution of liquid concentration from GC/MS measurements at the indicated times for operation at a fixed tube temperature of 1313 K over a four hour interval. The increase of acetic acid concentration is evident, which is due to refluxing. The specific molar concentration is dependent on the volume of the liquid containment and the conversion rate of ethyl acetate. The concentration of acetic acid developed from a heater of fixed size in an arbitrarily large volume of ethyl acetate would be small. The preferential vaporization of dissolved components will create the potential for them to decompose as they flow in the vapor film and are exposed to high tube wall temperatures.

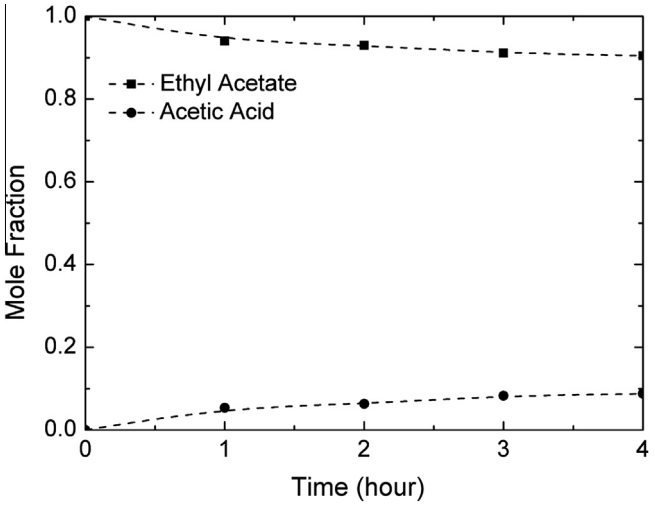

Fig. 5. Measured bulk liquid concentrations as a function of time for ethyl acetate and acetic acid at T_w = 1313 K over a four hour interval. Table 1 lists the additional species identified by GC/MS analysis in the liquid over this time interval.

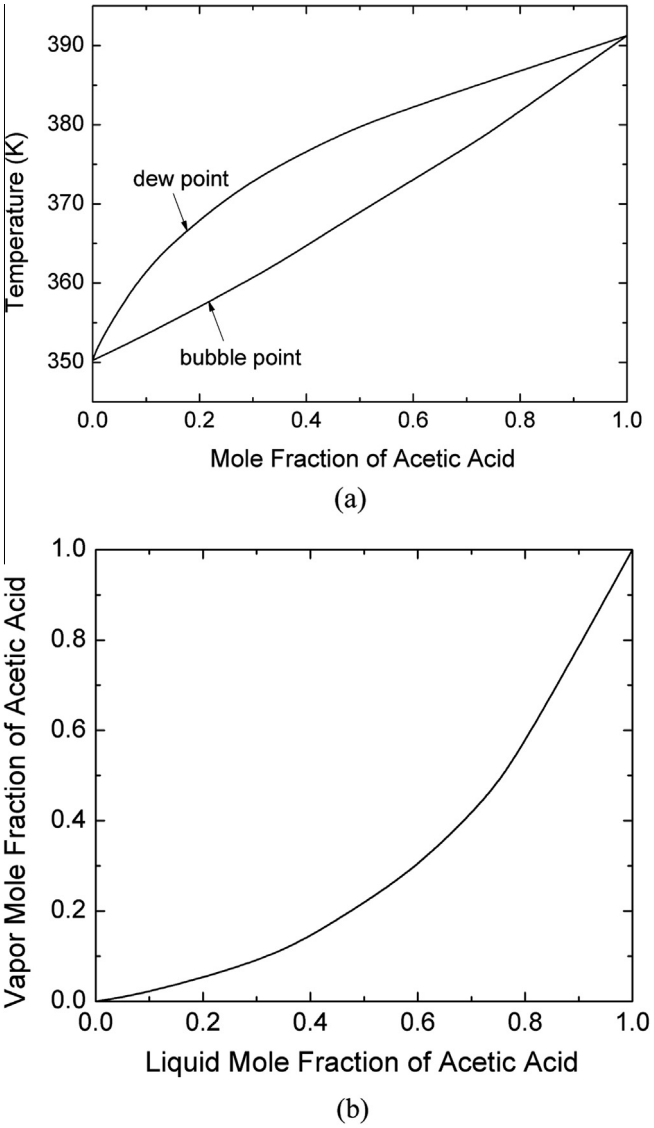

Fig. 6. (a) Variation of bubble and dew point temperatures with mole fraction of acetic acid at normal atmospheric pressure in a EA/acetic acid mixture [32]; (b) vapor mole fractions for indicated liquid mole fractions in the binary EA/acetic mixture.

The fractional amount of soluble products in the vapor film is determined by the phase equilibrium behavior of the mixture. Considering just a binary EA/acetic acid mixture, Fig. 6(a) shows the bubble point curve at atmospheric pressure and Fig. 6(b) illustrates the variation of vapor mole fraction in equilibrium with the indicated liquid composition in solution [32]. In reality, there may be many more condensable species formed, and Table 1 illustrates the suite of chemicals detected by GC/MS analysis of the liquid at a tube wall temperature of 1313 K along with the normal boiling points of the species. It is clear that the dominant condensable product species is acetic acid. At this particular tube wall temperature the liquid mole fraction of acetic acid was found to be 0.0533. According to Fig. 6(b), the vapor mole fraction would be about 0.01.

The decomposition of acetic acid may form carbon dioxide and methane,

$$CH_3COOH \xrightarrow{K_2} CO_2 + CH_4 \quad (4)$$

with K_2 known [33–36]. The extent to which Eq. (4) contributes to the overall decomposition process depends in part on detecting the three non-condensable gases carbon monoxide, methane and

Table 1
Liquid composition (mole fraction) at the indicated times for T_w = 1313 K.

Chemical	Formula	T_b [K]	1 h	2 h	3 h	4 h
Ethene	C_2H_4	169.4	0.0003	0.0003	0.0003	0.0003
Acetaldehyde	C_2H_4O	293.9	0.0005	0.0005	0.0005	0.0005
Ethanol	C_2H_6O	351.5	0.0002	0.0004	0.0003	0.0003
Acetone	C_3H_6O	329.3	0.0004	0.0003	0.0003	0.0003
3-Penten-1-yne	C_5H_6	317.2	0.0001	0.0001	0.0000	0.0000
Ethyl Acetate	**$C_4H_8O_2$**	**350.2**	**0.9405**	**0.9296**	**0.9108**	**0.9045**
Acetic Acid	**$C_2H_4O_2$**	**391.2**	**0.0533**	**0.0631**	**0.0825**	**0.0876**
Propanoic acid	$C_3H_6O_2$	414.0	0.0011	0.0015	0.0012	0.0012
Butane, 1-ethoxy-	$C_6H_{14}O$	364.7	0.0006	0.0010	0.0008	0.0012
Acetic Acid, anhydride	$C_4H_6O_3$	412.0	0.0027	0.0022	0.0027	0.0032
Heptane, 2-methyl-	C_8H_{18}	390.7	0.0005	0.0009	0.0005	0.0008

The significance of the bold characters is that these two chemicals are the main constituents of the bulk liquid.

ethylene in the product stream. Considering Eqs (3) and (4) as describing the overall conversion process, the complete conversion of EA may proceed through formation and decomposition of acetic acid and then ultimately to CO_2, CH_4 and C_2H_4,

$$CH_3COOC_2H_5 \xrightarrow{CH_3COOH} CO_2, CH_4, C_2H_4. \quad (5)$$

It should be noted that the concentration of acetic acid in the bulk liquid is dependent in part on the physical size (i.e., volume) of the chamber and its conversion rate. For an arbitrarily large containment volume or low conversion rate, the concentration of acetic acid in the liquid and, thus, in the vapor film would be small. Furthermore, if the condensate were flushed through the system and prevented from returning to the liquid pool, the reactant liquid would remain as a neat component regardless of the number of condensable species formed by decomposition. The influence of dissolved products on performance should therefore be viewed somewhat in the context of the experimental design.

4. Results

4.1. Boiling curve

The operational parameters of a reactor based on film boiling are defined by the so-called "boiling curve" of a liquid [37], which displays the relationship between the applied heat flux and the wall temperature over a spectrum of multiphase heat transfer modes. Fig. 7 shows the boiling curve of ethyl acetate measured in the present study. Four separate experimental runs are shown that illustrate the repeatability of the measurements. Each temperature shown in Fig. 7 is an average value at each power setting.

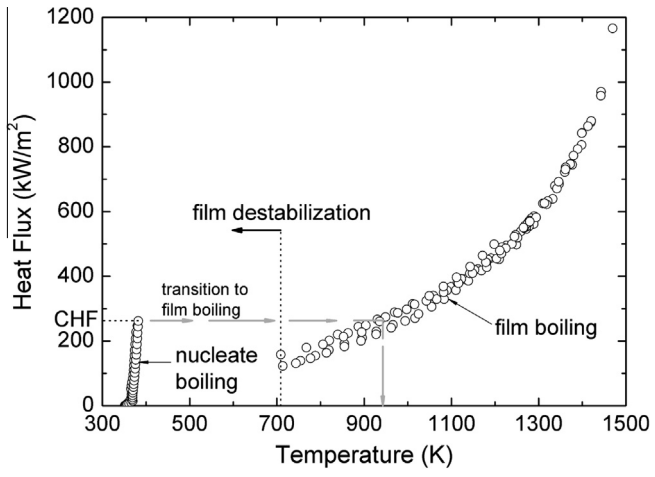

Fig. 7. Measured boiling curve of ethyl acetate. Thermal decomposition is confined to the film boiling domain. The arrows indicate the temperature excursion that occurs on transitioning from the critical heat flux (CHF) to the film boiling regime.

The boiling curve was developed with the tube initially submerged in the liquid pool, and the power then increased in steps. The nucleate boiling portion terminated at the CHF which was measured as approximately 253 kW/m^2 (at T_w 381 K). This value is within the range of predictions of correlations given by Lienhard [37] as corrected for the heater size, $q''_{CHF} = (0.89 + 2.27e^{-3.44\sqrt{R'}}) \times (0.131\rho_v^{1/2} h_{fg} \sqrt[4]{g(\rho_l - \rho_v)\sigma})$ where $R' = R\sqrt{g(\rho_l - \rho_v)/\sigma}$ which gives q''_{CHF} 282 kW/m^2 using the properties listed in Table 2 [38].

Above the critical heat flux (CHF), a wall temperature excursion occurs to transition the heat transfer mode to film boiling. For EA, the temperature jumped to about 940 K at this transition (note the arrows in Fig. 7). Because this temperature is well below Inconel's melting point, film boiling could easily be established on the tube when beginning with a submerged rod and heating it without danger of melt-down on the transition from CHF to film boiling. Once in film boiling, the average tube surface temperature is systematically adjusted to traverse the film boiling states. The low end is dictated by destabilization of the vapor film (about 711 K) and the upper temperature is limited by structural considerations of the tube as the melting point is approached. The practical range for the experiments reported here is between 711 K to about 1450 K. Over this range the gases flowing in the vapor film may decompose as discussed in Section 4.2.

Because the experiment employs input power as the control variable (rather tube temperature), the transition boiling portion of the boiling curve is not accessible, hence the gap in data for 381 K < T_w < 711 K, where the upper limit is the measured minimum film boiling temperature. Below this temperature, the bubbling instability of the transition region is not conducive to promoting pyrolysis, and the temperature in this regime is too low for significant product yields to be expected.

Fig. 8 shows a front view of film boiling of ethyl acetate at different times for ostensibly the same thermal condition of an average tube temperature of 1443 K. Mushroom-shaped bubble morphologies are evident. The configurations are highly stochastic and continually vary over time as the bubbles form and depart from the top of the tube. The bubbles contain the reaction products and unreacted vapors.

4.2. Product yields and gas and liquid compositions

The boiling curve and the images shown in Figs. 7 and 8 offer no substantive clue of reactions in the vapor film. The exhaust gas flow rate and chemical analysis of the gas stream provides the direct evidence of a particular decomposition route (cf, Eqs. (3) and (4)).

Fig. 9 shows the variation of exhaust gas flow rate (i.e., the "product yield") of ethyl acetate with average tube surface

Table 2
Selected properties under standard conditions unless otherwise indicated [38].

Chemical	Molecular Formula	MW [kmole/kg]	T_b [K]	ρ_l [kg/m^3]	ρ_v [kg/m^3]	h_{fg} [kJ/kg]	σ [N/m]	H_c [kJ/kg]
Ethyl Acetate	$C_4H_8O_2$	88.106	350.3	900; 826.17(T_b)	3.57; 3.02(T_b)	404.06; 365.52(T_b)	0.0234; 0.0173(T_b)	25400
Acetic Acid	$C_2H_4O_2$	60.052	391.1	1045	2.50	389.00	0.0271	14560

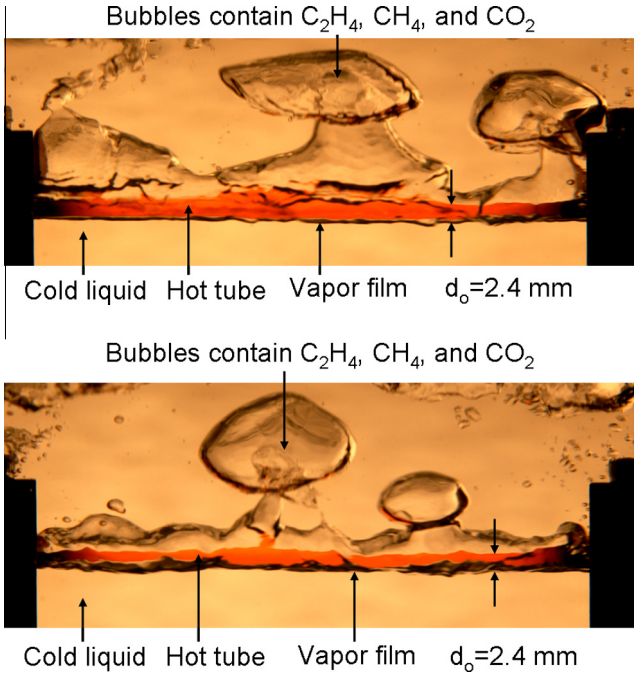

Fig. 8. Flash photographs of film boiling surrounding the tube at two different times. The liquid is ethyl acetate maintained at close to its boiling point and the average tube temperature is 1443 K.

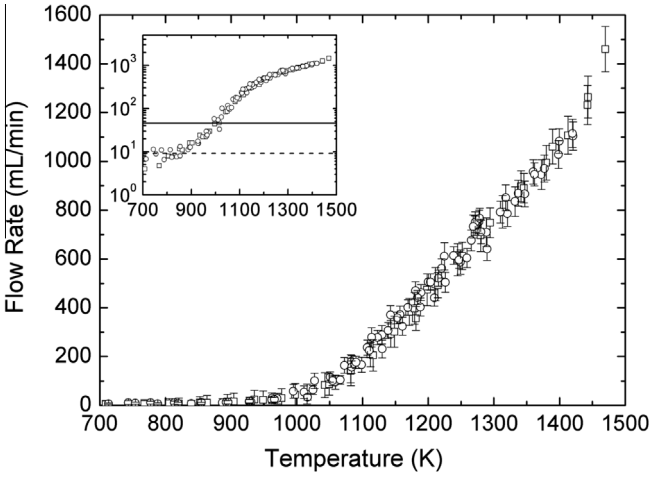

Fig. 9. Product yields as a function of tube temperature. Inset shows the same data on a logarithmic scale. The solid line and dashed line indicate the detection limits of flow meter FMA-A2309 and FMA-4310.

temperature. The flow rates were obtained from the flow meter voltage output by converting raw voltage signals to flow rate with the aid of a calibration as discussed in Appendix A. The simplicity of ethyl acetate decomposition (Eq. (5)) facilitated this conversion as the only non-condensable product gases in the exhaust stream are ethylene, methane, and carbon dioxide while acetic acid is condensed and returned to the liquid pool. A voltage-to-flow-rate conversion is only needed for these three gases.

The tube wall temperature is used as a representative value to define the reaction conditions though other temperatures could have been used. This assumption is based on the significant temperature drop that occurs across the vapor film. The conversion rates for the decomposition reactions discussed in Section 3 are expected to follow Arrhenius kinetics, $K \propto \exp(-E_a/\bar{R}T)$. Because the highest gas temperature is at the tube surface, the conversion rate is highest there for $T \approx T_w$ and it drops exponentially for $T < T_w$. The inset to Fig. 9 shows this sharp decline in the exhaust gas flow rate that is consistent with the strong dependence of the reaction rate on temperature. The solid line at 44 mL/min denotes the precision limit of the FMA-A2309 flow meter while the dashed line at 9 mL/min is the limit for the FMA-4310 flow meter. Below these levels, the measurements are not reliable. In overlapping ranges the two flow meters gave virtually identical flow rates.

Three gases were detected in the exhaust stream: ethylene, methane and carbon dioxide. Fig. 10 shows the measured fractional amounts of these species as T_w is varied. Ethylene dominates the gas concentration up to about 1300 K indicating that Eq. (3) is the main conversion step even though acetic acid is in the vapor film (due to the preferential vaporization process discussed previously). At higher temperatures carbon dioxide and methane concentrations increase indicating the importance of acetic acid decomposition (Eq. (4)) in the overall conversion process. The increase in carbon dioxide and methane concentrations and the concomitant slight reduction of ethylene with temperature shown in Fig. 10 tracks with the increase of dissolved acetic acid in ethyl acetate due to refluxing noted in Fig. 5.

While Eqs. (3) and (4) are believed to be the primary route for EA decomposition by film boiling, GC/MS analysis of the liquid identified many more condensable products. For example, a list of the species detected in the liquid pool at T_w = 1313 K is given in Table 1. Considering the low levels of these additional species, Eqs. (3) and (4) are the primary decomposition routes for ethyl acetate by film boiling.

Since Eqs. (3) and (4) are unimolecular decomposition reactions, the law of mass action leads to the rate of formation of product species as [39], $\frac{dC_{pi}}{dt} = K C_R$. Unfortunately, this equation cannot be integrated because the molar concentration of EA and acetic acid in the exhaust gas was not measured in the experiment, as these species were condensed and allowed to reflux into the liquid pool. However, the reaction rates provide a further clue on which of Eqs. (3), (4) is likely to be dominant. From the available rate constants for Eqs. (3) and (4) [20–24,33–36] we can say with reasonable certainty that acetic acid decomposition should proceed at a slower rate than EA as both species are transported around the tube in the vapor film.

Fig. 11 shows the molar flow rate of the individual non-condensable gases ($\dot{n}_i$) in the exhaust stream. The $\dot{n}_i$ were computed from the measured total product yield data, $\dot{N}$ (the volumetric flow rate data in Fig. 9 ($\dot{V}$) converted to total molar flow rate by assuming the ideal gas behavior,$\dot{N} = \dot{V}\frac{P}{RT}$) and the mole fractions of the individual species in the exhaust stream (y_i, Fig. 10) as $\dot{n}_i = y_i\dot{N}$.

At low temperatures, the ethylene molar flow rate (produced from Eq. (3)) is several orders of magnitude higher than methane and carbon dioxide (Eq. (4)) in keeping with the higher rate constant and lower activation energy of EA decomposition [20–24,33–36] relative to acetic acid. The large difference is main-

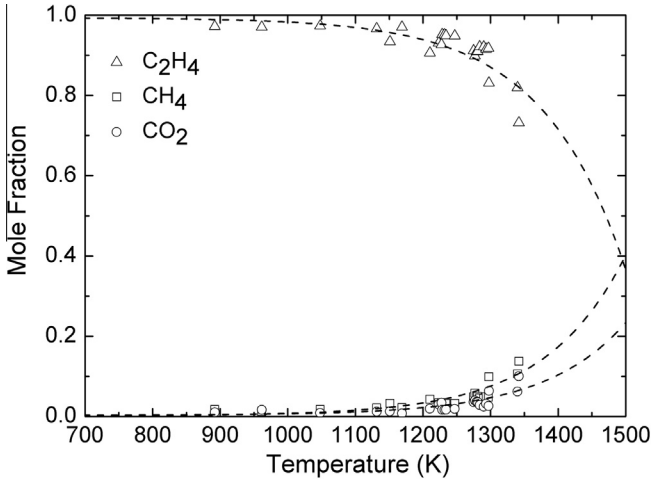

Fig. 10. Measured product gas compositions as a function of tube wall temperature. Dotted lines are correlations based on Eq. (A.3) and Table 5.

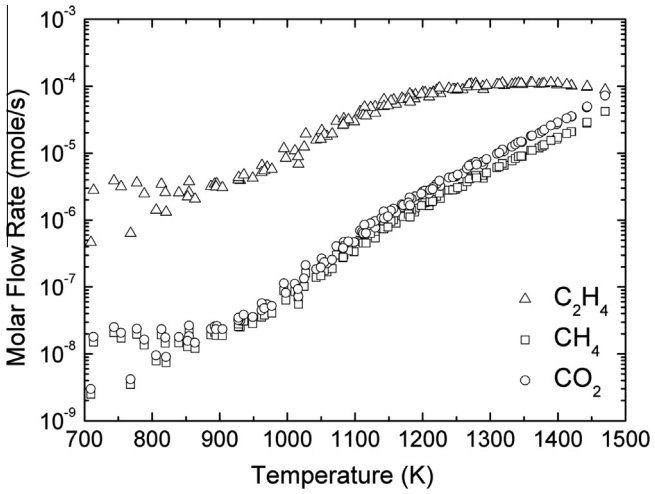

Fig. 11. Molar flow rate of the individual non-condensable gases.

tained for almost the entire temperature range investigated, except at the highest temperatures where the molar rates appear to converge. This trend is consistent with Fig. 10 which also shows negligible concentrations of the products of acetic acid decomposition at low tube temperatures and increasing concentrations of the acetic acid products at high temperatures. The concentration of methane and carbon dioxide track together throughout the temperature range as shown in Fig. 11 which is consistent with Eq. (4). This trend shows that the molar concentrations (and hence the molar flow rates of these two species) should be equal.

A final point to note regarding decomposition of organic molecules by film boiling is the potential for surface (catalytic) effects in the conversion process and the formation of a carbonaceous layer on the tube. The fact that the highest temperature in the vapor film occurs at the tube surface, with a steep drop in temperature to the liquid/vapor interface, and that the tube material itself (being a nickel alloy in the present experiments) could be catalytic suggest this possibility.

Some of the product gases detected in the present experiments are involved with reactions that can produce carbonaceous materials (e.g., CH_4 or CO_2 reacting with H_2). Interestingly, carbon formed during film boiling is the basis of an industrial process for synthesizing carbon composites from porous substrate preforms (e.g., cyclohexane is a common feedstock for this purpose [40–42]). Formation of a thin carbon layer was noted in a study of aqueous ethylene glycol mixtures [19,30], and it was observed in the present experiments as well.

The mechanism by which carbon deposits on the tube is unclear. Chemisorption of radicals at active sites on the solid surface can promote nucleation of solid aggregates that grow to form pyrolytic carbon layers. If such sites are not present, or only in a low concentration, the radicals will react with stable species in the gas phase and either produce soot precursors or participate in steps that lead to such additional species as CO, C_2H_2, C_2H_4, H_2 etc., though we have no evidence of homogeneous production of soot for the conditions of the present investigation. Once formed on a metal surface, a thin carbon layer could insulate the underlying metal from the gases flowing around it so that the potential for surface reactions catalyzed by the underlying metal may be diminished.

5. Conclusions

The conclusions of this study are the following:

(1) The thermal decomposition of ethyl acetate by film boiling resulted in formation of acid and ethylene in proportions consistent with a unimolecular decomposition process;
(2) For the experimental design of the present study in which acetic acid was allowed to reflux to the liquid pool, acetic acid further decomposed (along with ethyl acetate) to form methane and carbon dioxide, with product concentrations increasing with tube surface temperature;
(3) Over the temperature range investigated the concentrations of dissolved species other than acetic acid was small, indicating that ethyl acetate and acetic acid dominated the conversion process;
(4) Development of a carbon film on the tube surface was noted which was considered to mitigate the potential for surface catalytic reactions on the bare Inconel support;
(5) The remarkable consistency of the results presented suggest value for film boiling to not only promote chemical change of an organic liquid but to use the results to understand the decomposition kinetics involved.

Acknowledgments

This work was supported by National Science Foundation under Grant No. CTS-0933521. We thank Dr. Xia Zeng of Cornell University for his assistance with the GC/MS analysis of liquid samples and Mr. Eric Ching of Cornell for his help with the calibration process.

Appendix A.

The conversion of voltage from flow meter output to flow rate requires a voltage-to-flow rate calibration ($\dot{S}_i$). There are three molecules to consider in the calibration: C_2H_4, CO_2 and CH_4. The

Table 3
Correlation constants Eq. (A.2) for flow meter FMA-4310.

Chemical	$0 < \dot{S}_i$ [mL/min] $\leqslant 200$			$200 < \dot{S}_i$ [mL/min] $\leqslant 2000$		
	a_i	b_i	c_i	a_i	b_i	c_i
C_2H_4	−0.55	240.65	−2.62	8.69	222.75	7.66
CO_2	−3.84	292.85	−4.00	8.71	278.52	0.16
CH_4	−26.22	324.30	−7.27	9.54	279.98	11.94

Table 4
Calibration constants Eq. (A.2) for flow meter FMA-A2309.

Chemical	$0 < \dot{S}_i$ [mL/min] $\leqslant 200$			$200 < \dot{S}_i$ [mL/min] $\leqslant 2000$		
	a_i	b_i	c_i	a_i	b_i	c_i
C_2H_4	975.97	874.47	−0.68	17.38	1080.08	0.69
CO_2	−309.13	1575.86	−24.58	−69.22	1490.43	−17.46
CH_4	−2414.10	2002.09	−42.55	3.62	1463.91	−12.30

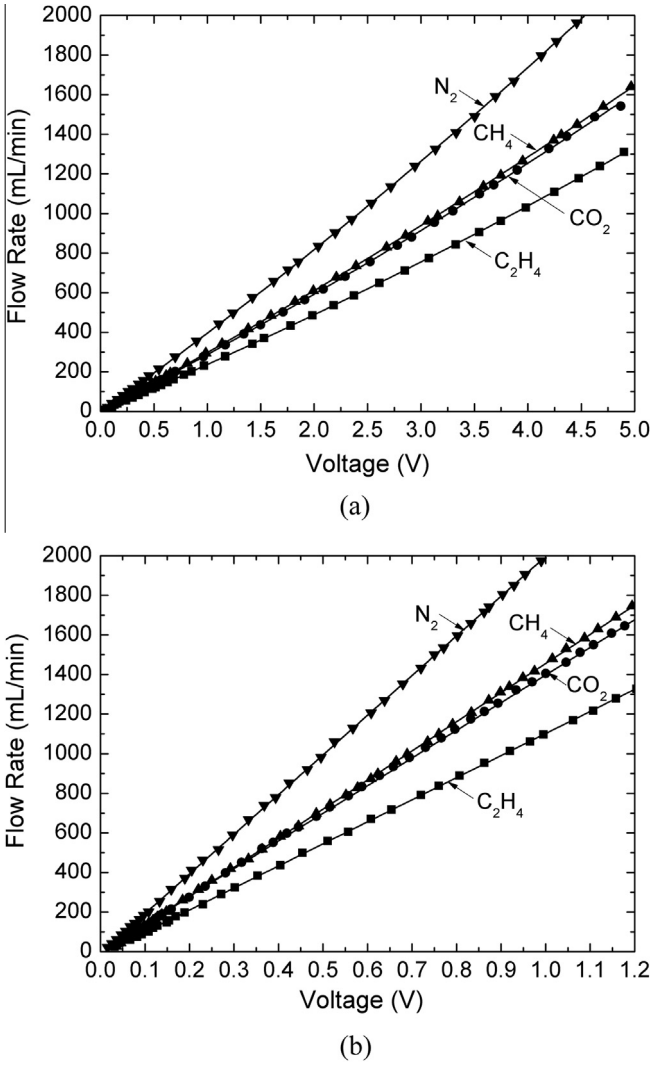

Fig. A1. Calibration curves of flow meters (a) FMA-4310 and (b) FMA-A2309. Correlation constants (lines in the figure) and equations are given in Eq. (A.2) and Tables 3 and 4.

relationship between the exhaust gas volumetric flow rate ($\dot{V}$, mL/min), or total product yield (Fig. 9) and the voltage output from the digital flow meters is

$$\dot{V} = \sum_{i=1}^{N} y_i \dot{S}_i \tag{A.1}$$

where y_i is the mole fraction of component i in the gas mixture and the $\dot{S}_i$ represent the relationship between the mixture component flow rates (mL/min) and flow meter voltage outputs. The $\dot{S}_i$ were correlated with flow meter voltage outputs (V) for the individual components detected in the exhaust stream using a quadratic relationship

Table 5
Correlation constants for product species mole fractions shown in Fig 10, $y_i = A_i \exp(T/B_i) + C_i$.

Chemical	A_i	B_i	C_i
C_2H_4	-5.99×10^{-7}	107.01	0.988
CO_2	1.75×10^{-7}	105.30	0.005
CH_4	1.94×10^{-7}	102.01	0.006

$$\dot{S}_i = a_i V^2 + b_i V + c_i \tag{A.2}$$

The calibration constants for the flow meters used (a_i, b_i, c_i) are listed in Tables 3 and 4. Fig. A1 shows the (near linear) correlations. A quadratic polynomial fitting gave a slightly more accurate calibration relation.

The component mole fractions in the exhaust stream y_i were determined from GC analyses. Fig. 10 previously presented the data. They were correlated as

$$y_i = A_i \exp(T/B_i) + C_i \tag{A.3}$$

where the constants are listed in Table 5 based on the data in Fig. 10. The dotted lines show the trends from Eq. (A.3) for the individual species.

References

[1] D.K. Liguras, D.I. Kondarides, X.E. Verykios, Appl. Catal. B: Environ. 43 (2003) 345–354.
[2] R. Seiser, L. Truett, D. Trees, K. Seshadri, Proc. Combust. Inst. 27 (1998) 649–657.
[3] K. Seshadri, T. Lu, O. Herbinet, S. Humer, U. Niemann, W.J. Pitz, R. Seiser, C.K. Law, Proc. Combust. Inst. 32 (2009) 1067–1074.
[4] P. Dagaut, S. Gail, M. Sahasrabudhe, Proc. Combust. Inst. 31 (2007) 2955–2961.
[5] D.A. Goetsch, L.D. Schmidt, Science 271 (1996) 1560–1562.
[6] D.A. Hickman, L.D. Schmidt, Science 259 (1993) 343–346.
[7] T. Aicher, L.J. Griesser, J. Power Source 165 (2007) 210–216.
[8] J.J. Krummenacher, K.N. West, L.D. Schmidt, J. Catal. 215 (2003) 332–343.
[9] R. Subramanian, L.D. Schmidt, Angew. Chem. Int. Ed. 302–305 (2005).
[10] G.J. Panuccio, B.J. Dreyer, L.D. Schmidt, AIChE J. 53 (2007) 187–195.
[11] J.R. Salge, B.J. Dryer, P.J. Dauenhauer, L.D. Schmidt, Science 314 (2006) 801–804.
[12] S. Chandra, C.T. Avedisian, in: Proc. R. Soc. Lond. A 432 (1991) 13–41.
[13] C.T. Avedisian, J. Koplik, Int. J. Heat Mass Transfer 30 (2) (1987) 279–293.
[14] S. Chandra, C.T. Avedisian, Int. J. Heat Mass Transfer 35 (1992) 2377–2388.
[15] M.J. Varady, Fuel reformation and hydrogen generation in direct droplet impingement reactors, Ph.D. Thesis, School of Mechanical Engineering, Georgia Institute of Technology, December, 2010.
[16] B.J. Urban, C.T. Avedisian, W. Tsang, AIChE J. 52 (2006) 2582–2595.
[17] C.T. Avedisian, W. Tsang, T. Davidovits, T.J.R. Allaben, AIChE J. 54 (2008) 575–581.
[18] S.R. Choi, J.W. Evangelista, C.T. Avedisian, W. Tsang, Int. J. Heat Mass Transfer 54 (2011) 500–511.
[19] J.W. Evangelista, C.T. Avedisian, W. Tsang, Int. J. Heat Mass Transfer 55 (2012) 6425–6434.
[20] A.T. Blades, Can. J. Chem. 32 (1954) 366–372.
[21] A.T. Blades, P.W. Gilderson, Can J. Chem. 38 (1960) 1407–1411.
[22] J.C. Scheer, E.C. Kooyman, F.L.J. Sixma, Recueil des Travaux Chimiques desPays-Bas 82 (11) (1963) 1123–1154.
[23] A.S. Gordon, W.P. Norris, J. Phys. Chem. 69 (1965) 3013–3017.
[24] W. Tsang, J.A. Walker, W. Braun, J.T. Herron, Chem. Phys. Lett. 59 (3) (1978) 487–491.
[25] A. Sakurai, M. Shiotsu, K. Hata, J. Heat Transfer 112 (1990) 430–440.
[26] A. Sakurai, M. Shiotsu, K. Hata, J. Heat Transfer 112 (1990) 441–450.
[27] X.S. Chou, L.C. Witte, J. Heat Transfer 117 (1995) 167–174.
[28] X.S. Chou, S. Sankaran, L.C. Witte, J. Heat Transfer 117 (1995) 175–178.
[29] Y.Q. Zhou, J.W. Rose, Int. J. Heat Mass Transfer 39 (1996) 3187–3191.
[30] J.W. Evangelista, An experimental demonstration of converting organic liquids and their aqueous solutions in a film boiling reactor, M.S. Thesis, Sibley School of Mechanical and Aerospace Engineering, Cornell, University, 2010.
[31] Special Metals Corp. Inconel Alloy 600. Publication Number SMC-027.(http://www.specialmetals.com/documents/Inconel%20alloy%20600%20(Sept%202008).pdf) 2008.
[32] F.H. Garner, S.R.M. Ellis, C.J. Pearce, Chem. Eng. Sci. 3 (1954) 48–54.
[33] P.G. Blake, G.E. Jackson, J. Chem. Soc. B (1968) 1153–1155.
[34] P.G. Blake, G.E. Jackson, J. Chem. Soc. B (1969) 94–96.
[35] J.C. Mackie, K.R. Doolan, Int. J. Chem. Kinet. 16 (5) (1984) 525–541.
[36] C.H. Bamford, M.J.S. Dewar, J. Chem. Soc. (1949) 2877–2882.

[37] J.H. Lienhard, A Heat Transfer Textbook, Prentice Hall, 1981. pp. 404–410.
[38] CRC Handbook of Chemistry and Physics. 92th ed. Taylor and Francis Group, LLC., 2011–2012. www.hbcpnetbase.com.
[39] F.A. Willams, Combustion Theory, Addison-Wesley, 1965. pp. 358–364.
[40] E. Bruneton, B. Narcy, B.A. Oberlin, Carbon 35 (1997) 1593–1598.
[41] D. Rovillain, M. Trinquecoste, E. Bruneton, A. Derre, P. David, P. Delhaes, Carbon 39 (2001) 1355–1365.
[42] K.J. Huttinger, Chem. Vap. Deposition 4 (1998) 151–158.